Current Density in a Model of a Human Body With a Conductive Implant Exposed to ELF Electric and Magnetic Fields

Blaž Valič,[1,2] Peter Gajšek,[1] and Damijan Miklavčič[2]*

[1]*Institute of Non-ionizing radiation, Ljubljana, Slovenia*
[2]*Faculty of Electrical Engineering, University of Ljubljana, Ljubljana, Slovenia*

A numerical model of a human body with an intramedullary nail in the femur was built to evaluate the effects of the implant on the current density distribution in extremely low frequency electric and magnetic fields. The intramedullary nail was chosen because it is one of the longest high conductive implants used in the human body. As such it is expected to alter the electric and magnetic fields significantly. The exposure was a simultaneous combination of inferior to superior electric field and posterior to anterior magnetic field both alternating at 50 Hz with the values corresponding to the ICNIRP reference levels: 5000 $V\,m^{-1}$ for electric field and 100 µT for magnetic flux density. The calculated current density distribution inside the model was compared to the ICNIRP basic restrictions for general public (2 $mA\,m^{-2}$). The results show that the implant significantly increases the current density up to 9.5 $mA\,m^{-2}$ in the region where it is in contact with soft tissue in the model with the implant in comparison to 0.9 $mA\,m^{-2}$ in the model without the implant. As demonstrated the ICNIRP basic restrictions are exceeded in a limited volume of the tissue in spite of the compliance with the ICNIRP reference levels for general public, meaning that the existing safety limits do not necessarily protect implanted persons to the same extent as they protect people without implants. Bioelectromagnetics 30:591–599, 2009. © 2009 Wiley-Liss, Inc.

Key words: numerical modeling; finite elements; dosimetry; implants; extremely low frequency exposure

INTRODUCTION

In modern medicine different implants are used for prosthetic, therapeutic, diagnostic, or experimental purposes [Dorland, 2000]. Due to markedly different dielectric properties of some implants in comparison to human tissue, electric, magnetic, and electromagnetic field distribution in a person bearing the implant is not the same as in a person without it.

The limit values of the electric and magnetic fields in an area with public access are proposed in various documents. Among them, one of the basic documents is the Guidelines for limiting exposure to time-varying electric, magnetic, and electromagnetic fields (up to 300 GHz) [ICNIRP, 1998]. When preparing ICNIRP Guidelines the authors focused on normal healthy humans without an implant which is explicitly stated: "Compliance with the present guidelines may not necessarily preclude interference with, or effects on, medical devices such as metallic prostheses, cardiac pacemakers and defibrillators, and cochlear implants. Interference with pacemakers may occur at levels below the recommended reference levels. Advice on avoiding these problems is beyond the scope of the present document but is available elsewhere [UNEP/WHO/

IRPA, 1993]" [ICNIRP, 1998]. However in the referred monograph (The environmental health criteria 137 Electromagnetic fields (300 Hz to 300 GHz) [UNEP/WHO/IRPA, 1993]) the problem of implants is only briefly mentioned in terms of cardiac pacemakers only.

ICNIRP Guidelines define two different types of limit values: basic restrictions and reference levels. Basic restrictions limit current density (head and trunk only) and specific absorption rate (SAR—the rate at

which energy is absorbed in body tissues, in $W\,kg^{-1}$) inside the human body and power density on the surface of the body to prevent negative effects to humans. Since these quantities in the body are difficult to measure and consequently compliance with basic restrictions limits is difficult to verify, reference levels were introduced. They are defined as electromagnetic quantities in the free space in absence of the human body: electric and magnetic field strength, magnetic flux density and equivalent plane wave power density. There are two principles linked to basic restrictions and reference levels. First, reference levels were set for the basic restrictions not to be exceeded. Second, if the reference levels are exceeded, it does not necessarily mean that the basic restrictions are also exceeded but this should be verified by more detailed analysis. These two principles are valid for a person without an implant. With the increasing number of implants, whether active or passive, in modern medicine an important question is raised and needs clarification: are these two principles valid also for a person with an implant? Can the implant alter the electric and magnetic field distribution inside the human body in such a way that the basic restrictions are exceeded in spite of the fact that reference levels are not?

In recent years this question was addressed in a number of reports. For example, McIntosh et al. [2005] calculated the SAR distribution and temperature change around a metallic plate in the head of an RF-exposed worker, and Virtanen et al. [2005] calculated the SAR enhancements due to the ring and rod shaped metallic implants at mobile frequencies. However, most of the papers deal with the RF fields, whereas we were unable to find any publication dealing with extreme low frequency (ELF) electric and magnetic fields.

In our study we used numerical modeling to calculate the current density distribution inside a human body with an intramedullary nail simultaneously exposed to an ELF (50 Hz) electric and magnetic field. As an implant we considered an intramedullary nail, used to fix broken cancelous bones, because it is one of the longest implants used in humans. It is thus expected to alter the current density distribution significantly. In addition to the intramedullary nail, the bones femur, patella, fibula, and tibia of the right leg were included in the model. Since the data of material properties in the literature are dispersed, we performed parameterization of the calculation with respect to the conductivity and permittivity of the soft tissue and bones. Under appropriate boundary conditions the electric and magnetic fields with the intensity corresponding to the reference levels for general public were simultaneously generated. To evaluate the influence of the implant, the current density distribution in the model with the implant was compared with the current density distribution in the model without the implant.

MATERIALS AND METHODS

The geometry of the model is based on female images from the Visible Human Data Set (VHDS) [The Visible Human Project, 2009]. We used female axial anatomical images with a resolution of 0.33 mm. Each of the 5186 images consists of 2048×1216 pixels with 24 bit color depth.

Because of its comprehensiveness and accessibility VHDS is widely used for numerical modeling, especially in the Finite Difference Time Domain calculations (FDTD) [Taflove, 1980]. However, the FDTD code is limited to high frequency. In some of the program packages for FDTD calculations, algorithms for low frequency calculations are also included, but the computer system and program package needed for calculation with adequate resolution are expensive. We therefore decided to use a Finite Element Method program package Comsol Multiphysics (Comsol, Stockholm, Sweden). This means we had to simplify the geometry sufficiently to make the mesh generation and the calculation possible.

First we decided which tissues to include in the model. By increasing the number of tissues we include in the model, the solution is more detailed. However, since each tissue is modeled as an object in the model, this means that the mesh becomes denser and more complicated in the model with many different tissues. We therefore decided to include only soft tissue for the whole model and bones in the region where the implant is situated. We included femur, patella, tibia, and fibula in the right leg. Soft tissue was separated in seven objects: head, upper and lower part of the torso, two arms, and two legs. Building-up of each object started with a selection of images, used to define the geometry of the object. First, we selected every 150th image (the distance between the images being 5 cm) for each object and manually cleared (set to white) the surrounding of each desired object (tissue type) in each of the images used. All modified images were then processed by a custom-written algorithm, where the border of the object in each picture was replaced by a polyline (a multi-segment line) with a predefined number of nodes. All nodes of each polyline lie in one plane. We defined these planes as being parallel to the ground. The position of each polyline was defined from the position of the polyline on the corresponding image taking into account the image resolution. The height above the ground was defined by the name of the corresponding image (names of the images are based on the height
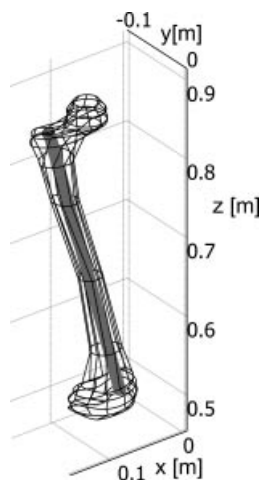
Fig. 1. Geometry of the right femur. The intramedullary nail is presented as a cylinder inserted in the femur.

above the ground). Using the Comsol Multiphysics function *loft* nodes in all polylines were connected to obtain a three-dimensional object. After the first iteration of an object generation, we analyzed it and included additional images in those *z* positions where the geometry was not sufficiently accurate. The final version of the femur is shown in Figure 1, where in each of the 15 images used to define the geometry of the femur, the border between the bone and surrounding tissue was presented by a polyline with 10 nodes.

Additional X-ray images were used to include the geometry of the implant. It would be straightforward to use anatomical images of patients with an implant for the entire model, but whole body images of an implanted patient were not available. As an implant we included an intramedullary nail, which is used to fix broken cancelous bones. The intramedullary nail was chosen for several reasons. It is implanted for a period of several months and is one of the longest high conductive implants used in the human body. Because of this we expected that it will have significant influence on the current density distribution. In addition, its upper end is in touch with soft tissue and is situated in the trunk (not in the limbs), from where ICNIRP basic restrictions are derived.

The geometry of the intramedullary nail was based on X-ray images of a woman with a broken right femur, taken after the fixation with an intramedullary nail. Images were taken at the Department of Traumatology (University Medical Centre, Ljubljana, Slovenia). Because of its simple shape, we presented the intramedullary nail together with the end cap as a cylinder with a diameter of 12 mm and a length of 365 mm. The position and orientation of the cylinder was defined by positioning the X-ray images in corresponding to the model of the femur, based on

VHDS images. The intramedullary nail inside the femur is shown in Figure 1. In the model, the intramedullary nail replaced part of the bone (not bone marrow), as bone was modeled as a homogeneous object. Intramedullary nails are made from different alloys; the most used are stainless steel (e.g., 316L [Carpenter, 2008]) and titanium alloys (e.g., Ti-6Al-7Nb [Synthes, 2007]). We selected a 316L stainless steel since its conductivity $1.35 \times 10^6 \ S \ m^{-1}$ [Upmet, 2007] is higher than the conductivity of the titanium alloys [Azom, 2007]. It is expected that higher conductivity will result in higher influence of the implant on current density distribution.

To define the region of calculation we enclosed the model of the whole human body in a block with the dimensions of 5 m $\times$ 5 m $\times$ 8 m. The model of the human body was positioned 3 cm above the bottom boundary, presenting a situation where the human is wearing shoes. Because of the large scale geometry of the model (the ratio between the smallest and the largest dimension in the geometry was more than 1:1000) the automatic mesh algorithm implemented in Comsol Multiphysics was unable to generate a mesh. By splitting the geometry into two geometries it was possible to decrease the ratio between the smallest and the largest dimension in the geometry. We did this as illustrated in Figure 2. Instead of one geometry we now have two: one geometry (large geometry) is a block with the dimensions of 5 m $\times$ 5 m $\times$ 8 m with a cut-out in the lower center part. This cut-out is a block with the dimensions of 0.5 m $\times$ 0.5 m $\times$ 2 m, the same as the second geometry (small geometry), in which the geometry of the human body is situated. In both geometries, after a minor correction of object geometries with special care for narrow regions, we were able to generate the mesh, but we still had to fine-tune the parameters of the mesh generation algorithm in the small geometries. The final mesh consisted of 12789 elements in the large geometry and 67605 elements in the small one.

We used the quasi-static electromagnetic application mode of the software package. This choice is valid if the largest dimension in the geometry is an order smaller than the wavelength of the electric and magnetic fields, in our case for frequencies of up to some megahertz. For the sinusoidal electric and magnetic fields, the system of equations which Comsol Multiphysisc uses for quasi-static electromagnetic application mode is as follows:

$$\nabla \times (\mu^{-1}\nabla \times \vec{A}) + (j\omega\sigma - \varepsilon\omega^2)\vec{A} + (\sigma + j\omega\varepsilon)\nabla V = \vec{J}_g \tag{1}$$

$$-\nabla \times ((j\omega\sigma - \varepsilon\omega^2)\vec{A} + (\sigma + j\omega\varepsilon)\nabla V - \vec{J}_g) = 0 \tag{2}$$

$$\nabla \vec{A} = 0 \tag{3}$$

where μ and ε are the permeability and permittivity of the material, $\vec{A}$ and V are the magnetic vector potential and the electric potential, respectively and $\vec{J}_g$ is the current density of sources. From the solution of $\vec{A}$ and V, electric field strength $\vec{E}$ and magnetic flux density $\vec{B}$ are calculated as

$$\vec{E} = -\nabla V - \frac{\partial \vec{A}}{\partial t} \qquad (4)$$

$$\vec{B} = \nabla \times \vec{A} \qquad (5)$$

To obtain the electric and magnetic fields with the values of reference levels for general public exposure at 50 Hz ($5000\ \mathrm{V\,m^{-1}}$ for electric field and 100 µT for magnetic flux density) given by ICNIRP Guidelines [ICNIRP, 1998], the required boundary conditions on the outer borders of the model were defined. On two opposite boundaries a voltage was applied to generate an electric field of $5000\ \mathrm{V\,m^{-1}}$, whereas the other four boundaries were set to insulation. By changing the active pair of the boundaries we changed the orientation of the applied electric field. Since all materials in the model have the same permeability (Table 1) and the current density in the model is very low (we can neglect the induced magnetic field due to the currents inside the human body), the magnetic field distribution inside the model is homogeneous. This simplified the calculation of the induced current density due to the magnetic field in the small geometry only. We defined the magnetic boundary conditions on the boundaries of the small geometry as 100 µT in the analyzed directions whereas for the electric field we defined identity boundary conditions on the corresponding boundaries in both large and small geometries. In this way, the large and small geometries are coupled for electric field during calculation and the obtained current density distribution is the same as if there was only one geometry composed of both large and small geometries.

Electromagnetic properties (Table 1) of the tissues included in the model were obtained from the existing literature [Gabriel et al., 1996a,b]. At 50 Hz the data in the literature is, however, highly dispersed, so we decided to perform parameterization for tissue conductivity and permittivity. We used two values for each parameter: soft tissue conductivity (0.2 and $0.4\ \mathrm{S\,m^{-1}}$) and permittivity (10^6 and 10^7) and bone conductivity (0.005 and $0.009\ \mathrm{S\,m^{-1}}$) and permittivity ($10^3$ and 10^4). Therefore, 16 calculations were performed altogether.

In order to compare the results and determine the influence of the intramedullary nail on the electric and magnetic field distribution inside the body we also calculated a model without the intramedullary nail. To be precise, in order to have the same geometry and mesh, we only changed electromagnetic properties of the intramedullary nail to correspond to those of the surrounding tissue, that is, the bone.

RESULTS

Using the Finite Element Method we calculated the current density distribution inside the human body with and without the implant exposed simultaneously to ELF (50 Hz) electric and magnetic fields. From the results for the big geometry (Fig. 2, left) it can be seen that the electric field is disturbed due to the presence of the human body. The boundary conditions define the unperturbed electric field strength with the value of reference level for general public exposure given by ICNIRP Guidelines ($5000\ \mathrm{V\,m^{-1}}$). Since the human body is a good conductor with respect to the surrounding air, the electric field strength inside the human body is very low (black, Fig. 2, right), but it increases in the area of air near and above the head (white). The values are more than $20000\ \mathrm{V\,m^{-1}}$, which is four times higher than in the unperturbed field. The magnetic field in the model is almost homogeneous as the value of the magnetic permeability of the materials in the model is 1 and the current densities in the model are low (thus the magnetic field due to the currents in the model is small compared to the external magnetic field).

The most important quantity to observe at low frequencies (up to 100 kHz) is the current density. This is also the value limited by ICNIRP Guidelines basic restrictions. At 50 Hz, the basic restriction for general

TABLE 1. Dielectric Properties of the Materials Included in the Model

Material	σ ($\mathrm{S\,m^{-1}}$)	ε_r	μ_r	References
Soft tissue	0.2; 0.4	10^6; 10^7	1	Gabriel et al. [1996a,b]
Bone	0.005; 0.009	10^3; 10^4	1	Gabriel et al. [1996a,b]
Air	0	1	1	
Intramedullary nail 316 L stainless steel	1.35×10^6	1	1	Upmet [2007]

Because of the dispersed data in the literature, we performed parameterization for tissue conductivity and permittivity. We used two values for each tissue.
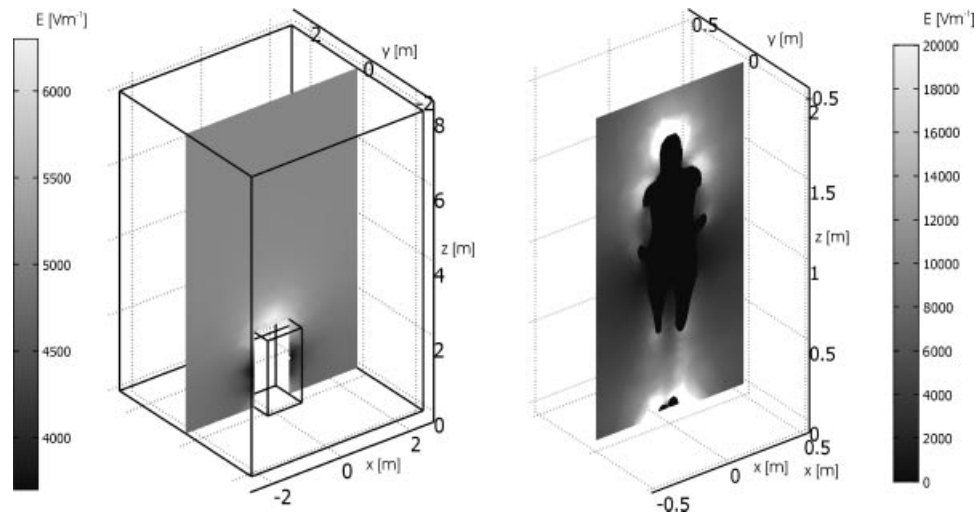
Fig. 2. From the electric field distribution for the exposure to the electric field (5000 V m^{-1}) in the inferior to superior direction and the magnetic field (100 μT) in the posterior to anterior direction in the large (left) and small (right) geometry it is clearly visible that the electric field distribution is altered by the human body. Instead of the homogeneous electric field (5000 V m^{-1}) in the whole model where no other objects are present, it is very low inside the human body (black), but quite high near and above the head. Note that the grayscale is in V m^{-1} and is different for left and right parts of the figure.

public for current density in the head and the trunk is 2 mA m^{-2}. However, according to ICNIRP Guidelines, current density should be averaged over a cross-section of 1 cm^2 perpendicular to the current direction. We were determining the current density in the transverse plane (parallel to the ground) 5 mm above the intramedullary nail. In this plane, direction of the current above the implant was perpendicular for all analyzed orientations and combinations of electric and magnetic fields. Table 2 presents 1 cm^2 average current density distribution for different orientations and combinations of the electric and magnetic fields. In our model, tissue conductivity and permittivity were 0.4 S m^{-1} and 10^6, respectively, bone conductivity was 0.009 S m^{-1} and permittivity 10^3. The implant was modeled as the 316L stainless steel (conductivity 1.35×10^6 S m^{-1}, permittivity 1). Besides the result of the models with the implant (fourth column), the results of the model without the implant are also given (fifth column). The first three cases refer to the exposure to electric field only. It is evident that the vertical orientation of the electric field (z axis) leads to the highest current densities in the observed area, whereas the most interesting directions for the exposure to magnetic field only (cases 4–6) are the posterior to anterior direction (y axis) and the left to right direction (x axis). In the last six rows of Table 2 the results of simultaneous exposure to both the electric and magnetic field are given for vertical electric field orientation. We can see that the results of simultaneous exposure are not just the sum of

the results of the exposure to the electric and magnetic fields, that is, the current density distribution has to be summed as a vector, not as a scalar. For example, in case 9 the result is a sum of the results in cases 3 and 5, whereas in case 10 the result is the difference between

TABLE 2. The 1 cm^2 Averaged Current Density in Soft Tissue 5 mm Above the Implant for Different Orientation and Combination of the Electric and Magnetic Field (Case) Is Presented

Case no.	E field	B field	Current density (mA m^{-2}) Implant	No implant
1	x	/	1.5	<0.1
2	y	/	1.3	<0.1
3[a]	z	/	4.8	0.3
4	/	x	1.8	0.3
5[a]	/	y	5.1	0.7
6	/	z	0.8	0.6
7[a]	z	x	3.7	0.3
8[a]	z	−x	6.0	0.5
9[a]	z	y	9.5	0.9
10[a]	z	−y	2.7	0.5
11[a]	z	z	5.8	0.6
12[a]	z	−z	5.6	0.7

The x direction is the left to right direction; the y direction is posterior to anterior direction, whereas the z direction is inferior to superior direction. Slash (/) indicates field absent, whereas minus (−) indicates 180° phase angle between the electric and magnetic field.
[a]Results exceeding ICNIRP basic restrictions (2 mA m^{-1}).
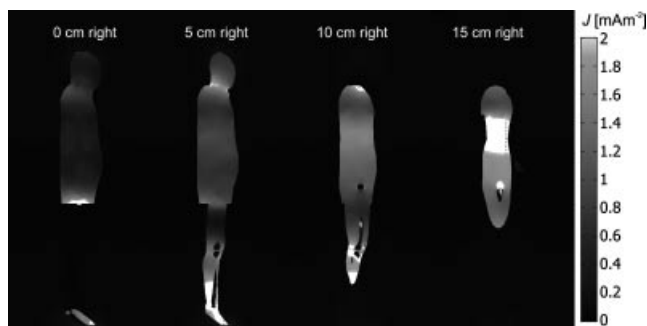
Fig. 3. The current density inside the human body with the implant in the median plane of the human body and in the sagittal planes 5, 10, and 15 cm to the right is shown for the worst-case situation: the electric field (5000 Vm^{-1}) in the inferior to superior direction and the magnetic field (100 μT) in the posterior to anterior direction. The grayscale is in mAm^{-2} and it covers the range from 0 to 2 mAm^{-2}, that is, ICNIRP basic restriction for general public exposure. Where the basic restriction is exceeded, white is used.

the results of cases 3 and 5. This means that in this case, the currents generated by the electric and magnetic fields are parallel, but oriented in opposite directions.

In Figure 3 the current density distribution in different sagittal planes is shown for the worst-case situation according to the results in Table 2: the electric field in the inferior to superior direction and the magnetic field in the posterior to anterior direction. We can see that most parts of the head and torso the current density is lower than the basic restriction for general public exposure given by ICNIRP Guidelines. In the legs below the knees the current density is higher than the basic restrictions (white, maximum 1 cm^2 average current density in this part of the body is 4.5 mA m^{-2}). This however is irrelevant according to ICNIRP Guidelines. To be precise, the current density is limited only in the head and trunk. Nevertheless, there are areas also in the trunk where basic restrictions are exceeded. On the right, where the current density distribution is shown in a sagittal plane 15 cm to the right there is a quite large white area in the upper torso, where 1 cm^2 average current density is between 2 and 3.5 mA m^{-2} and a smaller white area where the top of the intramedullary nail is in touch with soft tissue. The current density is also higher than the basic restriction; the maximum 1 cm^2 average current density in this part of the body is 9.5 mA m^{-2}. Because of low conductivity of the bones it can be seen that the current density inside the bones is low.

To determine the influence of conductivity and permittivity of soft tissue and bones on the current density distribution we performed parameterization. We calculated the current density distribution for all combinations of material properties in Table 1 for the

worst-case exposure situation, where the electric field is in the inferior to superior (z) direction and the magnetic field is in posterior to anterior direction (y). We found that the changes in the muscle and bone permittivity do not affect the results. The maximum 1 cm^2 average current density in the transverse plane (0.88 m above the ground) 5 mm above the implant remains the same: 9.5 mA m^{-2}. On the other hand, the conductivity of the bone and muscle is important. As can be seen from Table 3 and Figure 4 by increasing the conductivity of the bone, the area where the basic restrictions are exceeded remains unchanged (Fig. 4, compare the first row to the second and the third to the fourth). However, the maximum 1 cm^2 average current density in the model with the implant increases slightly with the increase of the conductivity of the bone (Table 3, compare the first row to the second and the third to the fourth). In the case of tissue conductivity of 0.2 S m^{-1} it increases from 8.2 to 8.3 mA m^{-2}, whereas in the model with tissue conductivity of 0.4 S m^{-1} it increases for <0.05 mA m^{-2} (in both cases it is 9.5 mA m^{-2}). The conductivity of the soft tissue affects the value of the current density as well as the area where the basic restrictions are exceeded. The higher the conductivity of the soft tissue, the higher is the current density and white area (Table 3 and Fig. 4, compare the first row to the third one and the second to the fourth one).

In the model without the implant, the current density in the same region is 0.6 mA m^{-2} for tissue conductivity of 0.2 S m^{-1} and 1.0 mA m^{-2} for tissue conductivity of 0.4 S m^{-1}. The increase of maximum 1 cm^2 average current density due to the implant is higher in the model with lower tissue conductivity (greater difference between the conductivity of the tissue and the implant), where maximum 1 cm^2 average current density is 12 times higher compared to the model without the implant. In the model with higher tissue conductivity this ratio is 10. This high

TABLE 3. The 1 cm^2 Averaged Current Density in the Soft Tissue 5 mm Above the Implant (Where the Influence of the Implant Is Maximal) for Different Material Properties of the Tissues Included in the Model

	Current density (mA m^{-2})	
Tissue conductivity (S m^{-1})	Implant	No implant
Soft tissue 0.2, bone 0.005	8.2	0.6
Soft tissue 0.2, bone 0.009	8.3	0.6
Soft tissue 0.4, bone 0.005	9.5	1.0
Soft tissue 0.4, bone 0.009	9.5	1.0

The electric field is in the inferior to superior direction and the magnetic field is in posterior to anterior direction which gives the worst-case situation (the highest values of the current density in the region above the implant, see Table 2).
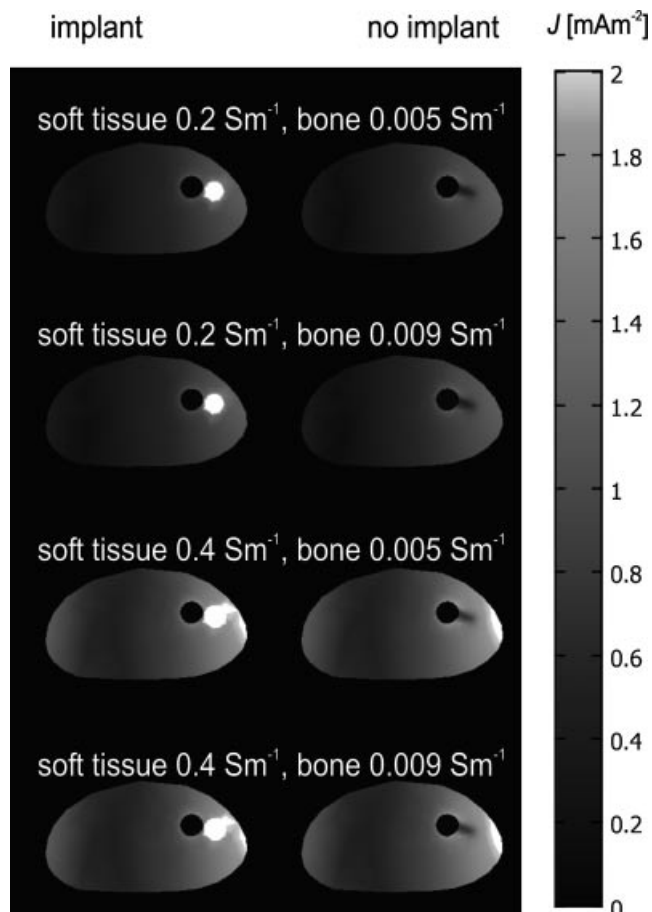
Fig. 4. The current density in the trunk is shown in the transverse plane 5 mm above the intramedullary nail (0.88 m above the ground) for different values of the soft tissue and bone conductivity for the worst-case situation: the electric field (5000 $V m^{-1}$) in the inferior to superior direction and the magnetic field (100 μT) in the posterior to anterior direction. The grayscale is in $mA\,m^{-2}$ and it covers the range from 0 to 2 $mA\,m^{-2}$, that is, ICNIRP basic restriction for general public exposure. Where the basic restriction is exceeded, white is used. For all combinations of dielectric properties the basic restriction is exceeded above the implant (white circular area), whereas for the higher conductivity of the soft tissue (0.4 $S\,m^{-1}$) it is exceeded also near the surface of the body. Black circular areas, where current density is very low represent the femur head.

Fig. 5. The current density in the transverse plane 0.3 m, 0.7 m, 0.88 m (5 mm above the intramedullary nail) and 0.92 m (45 mm above the femur) above the ground is shown for the worst-case situation: the electric field (5000 $V m^{-1}$) in the inferior to superior direction and the magnetic field (100 μT) in the posterior to anterior direction. The results for the model with the implant are in the left column, whereas for the model without the implant they are in the right column. The grayscale is in $mA\,m^{-2}$ and it covers the range from 0 to 2 $mA\,m^{-2}$, that is, ICNIRP basic restriction for general public exposure. Where the basic restriction is exceeded, white is used. This is either in the soft tissue in the lower part of the leg (first row), inside the implant (second row on the left) or in the tissue above the implant (third row on the left), and near the surface of the body (third and fourth row). Black circular areas, where current density is very low represent the bones.

factor demonstrates that the current density distribution is considerably affected by the implant. As seen in Figure 4 (right column), there is a small area where current density is higher than the ICNIRP basic restriction also in the model without the implant, in the case of high tissue conductivity (last two rows). However, the maximum 1 cm^2 average current density in this case is just a little over basic restrictions: 2.1 $mA\,m^{-2}$.

In Figure 5 the results of the model of a human with the implant (first column) are compared to the results of the model without the implant (second column) in different transverse planes. The results are given for the value of the soft tissue conductivity 0.4 $S\,m^{-1}$ and the value of the bone conductivity 0.009 $S\,m^{-1}$. Because a part of the total current in the leg now flows through the intramedullary nail, where the current density is high (small white area inside the black bone), we can see that the implant lowers the current density in the implanted leg (compare results for the right leg in the left and right panel of the second row). For example, maximum 1 cm^2

average current density in the tissue (not implant) in transverse plane 0.7 m above the ground is 1.5 mA m^{-2} for the model with the implant and 1.8 mA m^{-2} for the model without the implant. Inside bones the current density is low (they are black) as bones have low conductivity. In the third row the same results are shown as in the fourth row of Figure 4, while the last row presents the results for the plane only 4.5 cm higher at 0.92 m above ground. Comparing the left and right panel of the last row we can see that there are only minor differences between the results of both models with and without the implant only 4.5 cm away from the implant. This demonstrates that the influence of the implant is limited to the region where the implant is situated and that this influence fades quickly with distance.

DISCUSSION

Using numerical modeling we calculated the current density distribution in a model of the human body with and without an implant. We decided to calculate the current density distribution for ELF electric and magnetic exposure, because there are limited studies and reports dealing with ELF. The frequency of 50 Hz was chosen, as it is the power frequency used in most EU countries. However, for another common power frequency in the world, 60 Hz, the results are similar. ICNIRP basic restrictions for current density are 2 mA m^{-2} for both frequencies. At 50 Hz the ICNIRP reference level for magnetic flux density is 100 μT and for electric field strength it is 5000 V m^{-1}, whereas at 60 Hz, they are 20% lower at 80 μT and 4180 V m^{-1}. We should expect however that the induced and displacement current densities are 20% higher at 60 Hz for the same exposure as at 50 Hz; that is, if the material properties are the same (which is valid for so small a difference in frequency), the two effects cancel out. More importantly the effect of the implant on the current density distribution would be the same.

The presented results are for the general public basic restrictions and reference levels according to ICNIRP Guidelines. However, they could not be directly scaled to the occupational values since the ratio between the basic restrictions for occupational exposure and general public is 5, whereas for reference levels it is 5 only for magnetic flux density (reference levels for occupational exposure are 500 and 100 μT for general public exposure), but not for electric field strength (reference levels for occupational exposure are 10 and 5 kV m^{-1} for general public exposure).

Due to the restrictions of the software package only a limited number of objects were included in the model. In addition to the human body, composed of

head, upper and lower part of the torso and all four limbs, we only included the right leg bones: femur, fibula, patella, and tibia. With other numerical methods, based on a voxel model, it would be possible to include a larger variety of tissues. However, our approach is permissible as we only studied the local field distribution, which as demonstrated is only locally affected by the presence of the implant.

A limited number of included tissues meant that most of the human body was modeled as a homogeneous tissue with the conductivity of the muscle. Muscle conductivity is high compared to most of the other tissues thus the results of our model are conservative. This could explain why in Figure 3 (right) and Figure 5 ($z = 0.92$ m), current density is exceeding basic restrictions also in the upper part of the torso (regardless of whether or not the implant is presented in the model). For a less conservative model with lower tissue conductivity (0.2 S m^{-1} instead of 0.4 S m^{-1}), ICNIRP basic restrictions are no longer exceeded in the upper part of the torso. However, the effect of the implant on current density distribution still remains important, since it increases current density distribution in a limited volume by a factor of 10 or more.

Our results of modeling without the implant agree well with results from previous studies. For example, Gandhi et al. [2001] calculated the current density inside the human body exposed to 1 mT magnetic field at 60 Hz. The average layer current density inside the model was between 0.5 and 1 mA m^{-2}. Taking into account 10 times lower magnetic flux density in our model (100 μT), the results of our calculation are also 10 times lower: 0.021 mA m^{-2} in the area of the neck and 0.052 mA m^{-2} in the torso. The exposure of the human body in ELF 50 Hz electric field was also evaluated in Dimbylow [2000]. By scaling results from 1 to 5 kV m^{-1}, the maximum 1 cm^2 average current density in the muscle is 1.31 mA m^{-2}. The results obtained in our model are somewhat lower: 0.88 mA m^{-2}. Taking into account the simplifications of the geometry in our model, the results are in reasonable agreement.

CONCLUSION

Our results show that the intramedullary nail increases the current density in the area where the intramedullary nail is in touch with soft tissue. This increase is significant, since in spite of complying with ICNIRP reference levels for general public, the basic restrictions on current density for general public are exceeded. The region where significant increase in the current density is observed is, however, limited to less than 8 cubic centimeters, where the ICNIRP basic

restrictions are exceeded by a factor of two (current density higher than 4 mA m^{-2}). Except in the leg and in the part of the torso above the leg where an intramedullary nail is implanted, there is no observable difference in the current density distribution in other parts of the model.

The understanding of the electric and magnetic field distribution changes inside the human body due to conducting implants is not of interest to general public. However, cardiologists, traumatologists, and other physicians who implant such devices and patients receiving them should attach importance to the fact that the implant significantly alters the current density distribution inside the body. The current density might consequently exceed ICNIRP basic restrictions even though exposure is in compliance with ICNIRP reference levels.

ACKNOWLEDGMENTS

REFERENCES

Azom. 2007. The A to Z of Materials [Internet] Warriewood (Australia). [cited 2008 April 16]. Available from: http://www.azom.com.

Carpenter. 2008. BioDur Type 316LS Stainless [Internet] Reading (Pennsylvania USA). [cited 2008 August 30]. Available from: http://www.cartech.com.

Dimbylow PJ. 2000. Current densities in a 2 mm resolution anatomically realistic model of the body induced by low frequency electric field. Phys Med Biol 45:1013–1022.

Dorland IWA. 2000. Dorland's illustrated medical dictionary. Philadelphia, USA: Saunders.

Gabriel C, Gabriel S, Corthout E. 1996a. The dielectric properties of biological tissues: I. Literature survey. Phys Med Biol 41: 2231–2249.

Gabriel C, Law RW, Gabriel S. 1996b. The dielectric properties of biological tissues: II Measurements in the frequency range 10 Hz to 20 GHz. Phys Med Biol 41:2251–2269.

Gandhi OP, Kang G, Wu D, Lazzi G. 2001. Currents induced in anatomic models of the human for uniform and nonuniform power frequency magnetic fields. Bioelectromagnetics 22: 112–121.

ICNIRP. 1998. Guidelines for limiting exposure to time-varying electric, magnetic, and electromagnetic fields (up to 300 GHz). Health Phys 74:494–522.

McIntosh RL, Anderson V, McKenzie RJ. 2005. A numerical evaluation of SAR distribution and temperature change around a metallic plate in the head of a RF exposed worker. Bioelectromagnetics 26:377–388.

Synthes. 2007. Expert R/AFN Retrograde/Antegrade Femoral Nail, Technique Guide [Internet] Obderdorf (Switzerland): Synthes 2007. [cited 2008 April 16] Available from: http://www.synthes.com.

Taflove A. 1980. Application of the finite-difference time-domain method to sinusoidal steady state electromagnetic penetration problems. IEEE Trans EMC 22:191–202.

The Visible Human Project. 2009. [database on the Internet] Bethesda (Maryland USA): National Library of Medicine (US). [updated 2009 January 08, cited 2009 April 7]. Available from: http://www.nlm.nih.gov/research/visible/getting_ data.html Subscription required.

UNEP/WHO/IRPA. 1993. Environmental health criteria 137 electromagnetic fields (300 Hz to 300 GHz). Geneva, Switzerland: WHO.

Upmet. 2007. Stainless Steel 316L Technical data [Internet] Hamilton (Ohio USA). [cited 2008 April 16]. Available from: http://www.upmet.com.

Virtanen H, Huttunen J, Toropainen A, Lappalainene R. 2005. Interaction of mobile phones with superficial passive implants. Phys Med Biol 50:2689–2700.